1998

The *Oleander* Project: Monitoring the Variability of the Gulf Stream and Adjacent Waters between New Jersey and Bermuda

Hans Thomas Rossby
University of Rhode Island, trossby@uri.edu

E. Gottlieb
University of Rhode Island

Citation/Publisher Attribution

Rossby, T., & Gottlieb, E. (1998). The Oleander< Project: Monitoring the Variability of the Gulf Stream and Adjacent Waters between New Jersey and Bermuda. *Bull. Amer. Meteor. Soc.*, **79**, 5–18. doi: 10.1175/1520-0477(1998)0792.0.CO;2.
Available at: https://doi.org/10.1175/1520-0477(1998)079<0005:TOPMTV>2.0.CO;2

The *Oleander* Project: Monitoring the Variability of the Gulf Stream and Adjacent Waters between New Jersey and Bermuda

The *Oleander* Project: Monitoring the Variability of the Gulf Stream and Adjacent Waters between New Jersey and Bermuda

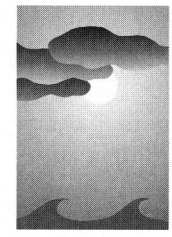

T. Rossby and E. Gottlieb
Graduate School of Oceanography, University of Rhode Island, Narragansett, Rhode Island

ABSTRACT

An overview of the first 4.5 years of operation of a program to monitor the structure and variability of the Gulf Stream (GS) is presented. A container vessel that operates on a weekly schedule between Port Elizabeth, New Jersey, and Hamilton, Bermuda, is equipped with a 150-kHz narrowband acoustic Doppler current profiler to measure currents from the surface to ~300 m depth. A major objective of the multiyear program is to study the annual cycle and interannual variations in velocity structure and transport by the GS. In this survey the focus is on the transport and lateral structure of the current at 52-m depth.

The velocity maximum is constant at 2.07 ± 0.24 m s^{-1} (4 kt) with a seasonal range of ~0.1 m s^{-1}. Seasonal and interannual variations in total transport are observed but appear to be limited to the edges of the current, apparently reflecting low-frequency variations in the intensity of the recirculating waters adjacent to the stream. The transport by the central core of the current, defined as those waters moving at 1 m s^{-1} or faster, equals 0.9×10^5 m^2 s^{-1}, has no seasonal signal, and is constant to within a few percent when averaged in half-year intervals. If the central core of the current is viewed as "insolated" from the effects of meandering, this result implies substantial stability to the large-scale wind-driven and thermohaline circulations during the observation program. Variations in poleward heat transport probably originate less in the GS and more from changing heat loss patterns at higher latitudes.

Other issues concerning the potential vorticity field and energy conversion rates are also discussed. This ongoing program illustrates the role commercially operated vessels can play in making repeat observations of the velocity structure (and other parameters) of the ocean on a regular basis.

1. Introduction

Flowing north offshore of North America, the narrow, swift Gulf Stream transports vast quantities of mass and heat from low to high latitudes, making it a major contributor in maintaining the global heat balance. Consequently, considerable interest has developed concerning the stability of these fluxes, because any change in either the temperature of Gulf Stream waters or the amount of water it transports may significantly impact the climate of the Northern Hemisphere. Although we perceive the Gulf Stream (GS) as a single current, it comprises two quite separate modes of ocean circulation. One mode, the wind-driven component, closes the anticyclonic circulation around the subtropical gyre driven by the westerlies at midlatitudes and the trade winds in the Tropics. The second, thermohaline mode represents the vertical overturning of the ocean driven by the meridional gradient of heating and cooling and resultant sinking of surface waters at high latitudes. How much of the waters transported by the stream belong to each of these modes, what is the nature of their coupling, how much do they vary with time, and on what timescales, are questions of fundamental importance for an improved understanding of the stream's role in regulating our climate, regionally and globally.

Countless satellite images of sea surface temperature have given us a clear overview of the mean path

Corresponding author address: Prof. T. Rossby, Graduate School of Oceanography, University of Rhode Island, Narragansett Bay Campus, Narragansett, RI 02882-1197.
E-mail: tom@rafos.gso.uri.edu
In final form 2 October 1997.

and meandering of the Gulf Stream, the exchange of waters between the stream and surrounding waters, and how warm and cold core rings form and break off from the current. From hundreds of hydrographic sections taken across the Gulf Stream since the *Challenger* section in 1873 we have learned much about the structure of the Gulf Stream and how its transport varies as a function of downstream distance (Knauss 1969; Halkin and Rossby 1985; Hogg 1992; Johns et al. 1995). Despite its permanence, the Gulf Stream evinces such variability that it has proven quite difficult to establish its mean transport with confidence, let alone how it varies on seasonal and longer timescales. Estimates thereof vary considerably; for example, Greatbatch et al. (1991), using the Levitus (1989) analysis of interpentadal variability of temperature and salinity in the North Atlantic, estimate that the Gulf Stream decreased its total (but primarily baroclinic) transport between the late 1950s and the early 1970s, approximately 30×10^6 m^3 s^{-1} or 30 Sv (sverdrups). Sato and Rossby (1994), on the other hand, obtain about a 6-Sv decrease in baroclinic transport (relative to a level of no motion at 2000 m) for the same period. Why these estimates differ so much needs careful assessment, but even a 6-Sv decrease of waters with a temperature difference of 16°C, for example, relative to the deep return flows (the thermohaline mode) would lead to an O(0.4 PW) reduction in heat transport at midlatitudes. Thus accurate knowledge of the Gulf Stream's mass transport and thermal structure, particularly of the fast-moving warm upper layers, plays an important role in a quantitative assessment of its and the ocean's role in the global heat balance. In addition, such knowledge provides an integral constraint on any analytical or numerical circulation model of the North Atlantic.

The combination of two relatively new technologies have enabled a fresh approach to the study of the Gulf Stream. The first one, the shipboard acoustic Doppler current profiler (ADCP), allows us to obtain high-resolution sections of upper-ocean currents from the surface to a few hundred meters relative to the moving vessel. The other, the Global Positioning System (GPS), gives very precise position information continuously. By subtracting the ship's velocity from the ADCP-measured velocity, we can determine ocean currents to an accuracy of better than 0.05 m s^{-1} from vessels under way at 15 kt (> 7 m s^{-1}) speeds.

This paper reports on the operation of an ADCP aboard the M/V *Oleander,* a container vessel that operates on a weekly schedule between Port Elizabeth, New Jersey, and Hamilton, Bermuda. This ongoing, twice-weekly sampling of the Gulf Stream, which has continued without serious interruption since early fall 1992, enables study of the variability of the Gulf Stream and surrounding waters over a wide range of timescales and for an extended period of time. The main interest centers on seasonal and interannual variations in upper-ocean mass transport and their impact on the poleward heat transport. The paper describes the observational program and details some of the results obtained to date, beginning with a few words about the ADCP principle of operation. The cover illustration indicates schematically the measurement program relative to the upper-ocean velocity and thermal structure.

2. Measuring currents from a fast-moving vessel

The ADCP works by repeatedly transmitting acoustic pulses of a certain frequency in four oblique directions (30° off the vertical) from beneath the ship. After each transmission it listens to the backscattered echoes from suspended particulate matter (primarily zooplankton) at various depths. By measuring the Doppler-shifted frequency of the reflected signal as a function of time, one obtains a vertical profile of relative motion between the ship and the water column along each of the acoustic beams. Next, assuming that the water moves in horizontal slabs, one can transform the along-beam velocity components into horizontal and vertical components of velocity relative to the ship. Last, by subtracting out the ship's velocity measured by the GPS navigation, one obtains the absolute ocean current velocity. The uncertainty in water velocity depends primarily on ship speed in the along-track direction and on ship heading in the cross-track direction. The accuracy of the ship's speed from GPS is typically 0.05 m s^{-1} when averaged over 20 min or more. Due to the high speed of the vessel the uncertainty of the gyrocompass is a much more serious concern, illustrated by the fact that a 1° heading error times 16 kt leads to an errant cross-track velocity of 0.14 m s^{-1}. Any compass error (and alignment error of the ADCP) can be determined directly in the shallow water over the continental shelf by computing the ship's track using the ADCP's so-called bottom track mode and comparing with the GPS-determined track; the difference between these yields an estimate of gyrocompass error. By repeating this check from many

transits across the continental shelf one obtains a very precise estimate of the mean and stability of the gyrocompass offset. Further, since the M/V *Oleander* steams on a constant heading for most of the transit, spurious so-called Schüler oscillations are kept to a minimum. Finally, since summer 1995 a special attitudinal GPS (AGPS) receiver that resolves ship's heading independent of the gyrocompass to less than 0.1° has been in operation.

The shallow draft of the vessel has led to one significant shortcoming of the ADCP operation, namely, the drawdown of bubbles at the bow in heavy weather and on northbound transits when the ship carries only a light load. The presence of bubbles severely attenuates both the transmitted and received signal, often rendering the ADCP useless. This problem might be reduced by attaching a cowling or dome around the ADCP opening, but this would interfere with the ship's operation and make drydocking more cumbersome. This limitation means that less than half of the southbound and a third of the northbound transits have complete coverage between the continental shelf and Bermuda. A number of other sections provide partial coverage, particularly in the north. The reader is referred to a paper by Flagg et al. (1998) for a complete technical discussion.

3. The velocity field

The four panels of Fig. 1 show a series of transects from August–September 1993 with the velocity vectors at 52 m superimposed on National Oceanic and Atmospheric Administration Advanced Very High Resolution Radiometer (NOAA AVHRR) maps of sea surface temperature (SST). The SST images reveal clearly the core of the GS, its meanderings through the surrounding waters, and the westward migration of a warm-core ring. The velocity vectors reflect the presence of the GS and various eddy motions to either side. Note the coincidence of the high-velocity jet of the GS with the band of warm surface waters; as the thermal band meanders, so does the jet. The cross-stream shape of the jet possesses a distinct asymmetric form with a narrow zone of sharp cyclonic shear to the north and a broader zone of anticyclonic shear to the south. As shall be seen later, the 2 m s^{-1} velocity maximum of the jet has a surprisingly small standard deviation, 0.24 m s^{-1}. The lateral shear depends significantly upon variations in the width of the current and/or interactions with the surrounding mesoscale eddy field. The warm, circular pattern and corresponding velocity vectors north of the GS reveal the presence of a warm-core ring drifting west across the ship's track. South of the stream the varying velocity vectors reveal eddy activity throughout the Sargasso Sea. Some of this activity could reflect cold-core rings whose SST signature has faded away. These panels emphasize two major properties of the GS,

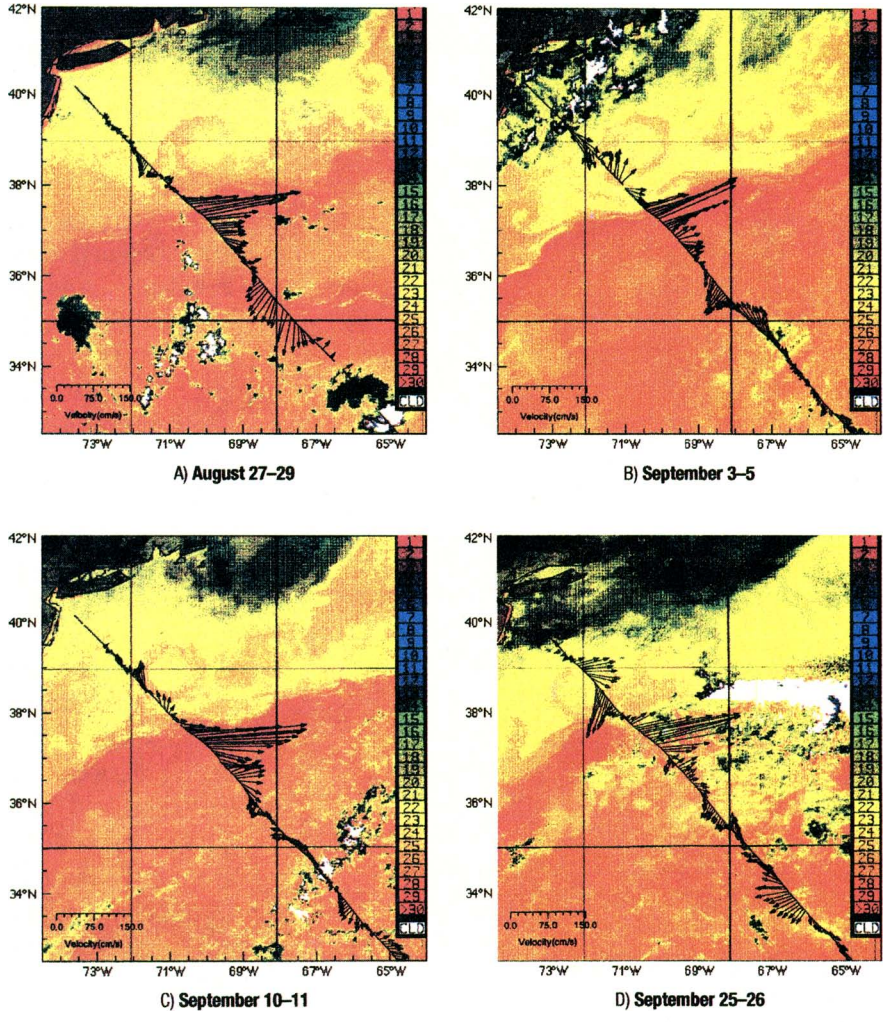

FIG. 1. Four transects from August–September 1993 with superimposed AVHRR SST.

namely, its permanence on the one hand and its path variability on the other.

The large velocity gradient (front) along the north edge of the GS does not necessarily coincide with the sharp thermal front there. It will be seen later that the thermal front can be displaced anywhere within about 100 km to either side of the velocity front. This results from the exchange of waters between the meandering stream and surrounding waters, that is, the expulsion or detrainment of warm water to the west and north of meander crests and the entrainment of cold waters into the high velocity zone of the current east or downstream of crests. [Another technical factor comes from the 48-h compositing of up to four SST images (done to remove the presence of clouds), which means that the ADCP section and SST images do not coincide perfectly in time.] The ADCP offers a very precise way to quantify the relationship between velocity and SST since it also records temperature (to be discussed below).

Over the depth range that the 150-kHz ADCP can operate, from the surface to 300+ m, currents exhibit a high degree of vertical coherence. The top and bottom panels in Fig. 2 show speed in the directions 75°T (T identifies a bearing from true north) and 165°T, that is, along and normal to the GS in the section in Fig. 1d. The contour interval is 0.2 m s^{-1}, and the white and gray areas denote regions of positive and negative flow, respectively. The upper panel reveals the GS core with peak speeds in excess of 1.8 m s^{-1}. Note the penetration of the sharp cyclonic shear on the northern side to several hundred meters depth and the weak and even reverse vertical shear on the southern side of the current. The variable depth of the contoured fields results from a number of factors: zooplankton density (acoustic backscatterers), sea state (entrainment of bubbles underneath the vessel), and ship speed (at certain speeds the ship apparently exhibits high noise levels). This means that ADCP coverage decreases rapidly with increasing depth, particularly south of the GS where zooplankton density is low. In wintertime the quality of the data decreases due to high sea states and low zooplankton populations.

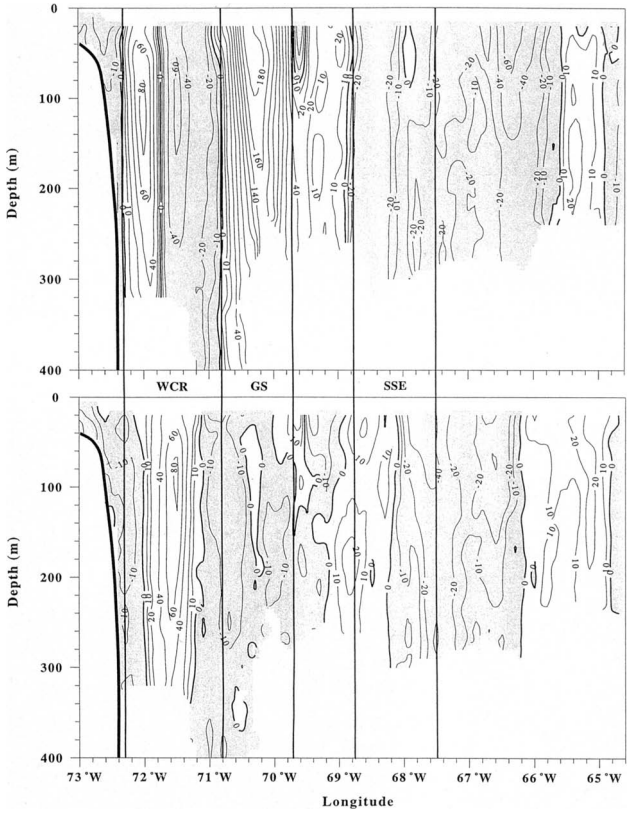

FIG. 2. Along-stream (75°T) and cross-stream (165°T) velocity components (top and bottom panels, respectively) from along the ship's track in Fig. 1d. The lines denote the warm-core ring, the Gulf Stream, and a Sargasso Sea eddy.

4. The mean field

From the 4.5 years of operations thus far, October 1992–March 1997, there are about 130 sections of good to high quality. Figure 3 shows the Eulerian mean velocity vectors and corresponding velocity variance ellipses plotted every 25 km along the mean path of the ship. The ship stays within a few tens of kilometers of its great circle path, justifying the projection of all data onto one line. Figures 3a–c show 1-yr subsets as indicated, while Fig. 3d shows the 4.5-yr grand average. The GS stands out clearly at all times in both the mean and variance fields, as does the flow to the west in both the Sargasso Sea and slope waters. But the latter also evince significant variations from year to year in their strength and shape. To both sides of the GS the flow is to the west, but in Figs. 3a and 3c, for example, there is a strong flow toward the GS from the southeast, indicating low-frequency variations on scales between that of the mesoscale eddy field, O(50 km), and the recirculating gyre itself, O(500 km). Close to Bermuda the mean flows are very weak. The spatially continuous sampling brings out another striking aspect, namely, the sharp decrease in velocity variance outside the GS and its further decrease toward Bermuda. The axes of the variance ellipses indicates the eddy kinetic energy (EKE) levels in J kg^{-1} defined as

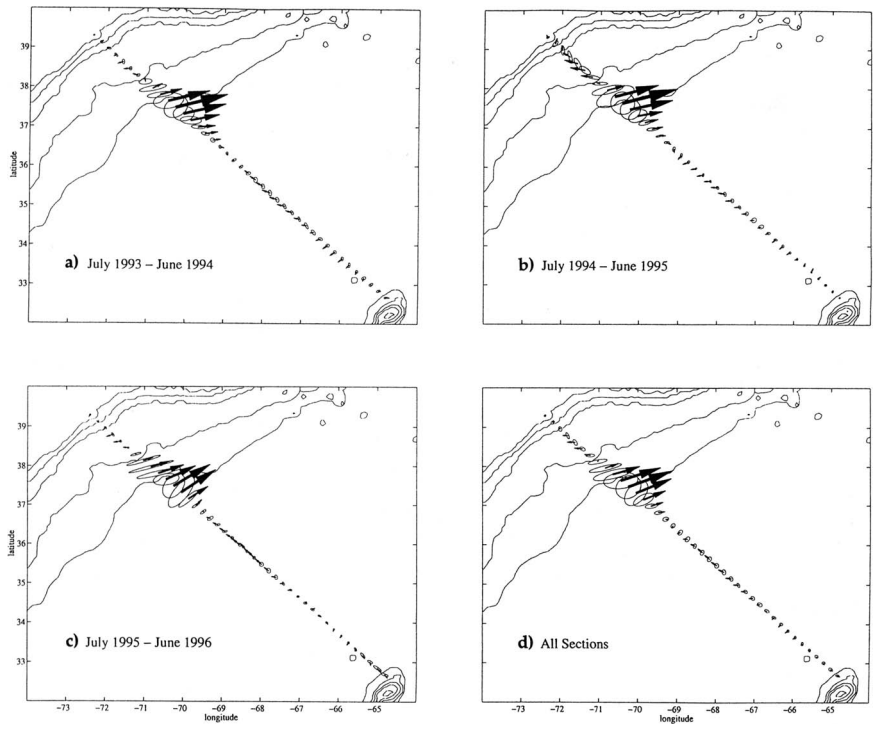

FIG. 3. Mean velocity vectors (1 m s^{-1} = 1°lat) and variance ellipses (1 J kg^{-1} = 1°lat). The panels correspond to the periods (a) July 1993–June 1994, (b) July 1994–June 1995, (c) July 1995–June 1996 and (d) October 1992–March 1997.

$$\mathrm{EKE} = 0.5\left(\overline{u'^2} + \overline{v'^2}\right),$$

where u' and v' represent departures from the local ensemble means along the track. The ellipticity and direction of the major axis indicate the degree of coupling between u' and v'. Only in the GS do we find strong coupling between the two; elsewhere their near roundness suggests a fairly isotropic eddy field. Between 36° and 33°N the average EKE drops from ~0.06 to ~0.03 J kg^{-1}. This 4.5-year dataset permits a very detailed analysis of the upper-ocean velocity field across the NW Atlantic.

The primary focus of this study concerns the long-term stability of the Gulf Stream itself. The simplest and in many ways most compact statement consists of a vector plot of all GS velocity maxima, shown in Fig. 4a. The vectors represent the single largest vector in the 36°–39°N band from all transits, north- or southbound. The mean of the velocity maxima, 2.07 m s^{-1} (= 4 kt), shows little dependence upon direction and has a remarkably small standard deviation, 0.24 m s^{-1} or 12% of the mean. (The circular arc represents 2.07 m s^{-1}.) Figures 4b–d show the velocity maximum (v_{max}) as a function of latitude, time of year, and as a function of time, revealing a surprising independence of v_{max} to three fairly obvious factors that might be considered. A slight seasonal dependence with a minimum in early winter does appear, but it accounts for only a small fraction of the variance (0.1 m s^{-1} range). The interyear mean and variance of v_{max} show no significant change. We will return to this below. The GS does exhibit one clear seasonal signal, namely, a migration south in spring and north in fall, Fig. 5a, but it accounts for only a small fraction of the total mesoscale meandering of the current. Figure 5b reveals significant interannual migration in latitudinal position. The cubic fit to the data in Fig. 5b was used to remove the low-frequency shifting prior to constructing the annual cycle in Fig. 5a.

Numerous studies in recent years have drawn attention to the structural stability or robustness of the GS itself (cf. Halkin and Rossby 1985; Hall 1986; Johns et al. 1995). The observations

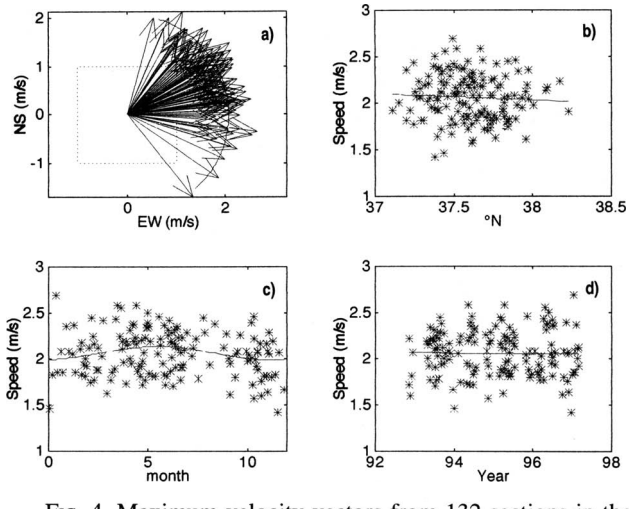

FIG. 4. Maximum velocity vectors from 132 sections in the latitude 37°–39°N from all transits, north- or southbound. The mean of the velocity maxima, 2.07 m s^{-1} (= 4 kt), shows no dependence upon direction and has a remarkably small standard deviation, 0.24 m s^{-1} or 12% of the mean. (b), (c), (d) The velocity maximum as a function of latitude, time of year, and time, respectively.

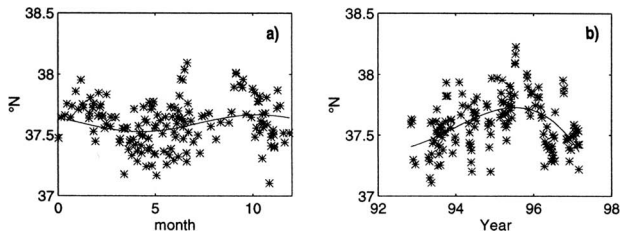

FIG. 5. Latitude of the velocity maximum as a function of (a) month and (b) time, including a cubic fit, which was used to removed interannual variations prior to constructing (a).

of the present program bear out those earlier results. Focusing on the lateral structure of the current, Fig. 6a shows the downstream component of motion, defined as the component parallel to the maximum velocity vector, as a function of distance normal to that vector. With the velocity maxima from all crossings positioned at $x = 0$, the asymmetry of the current becomes evident with sharp cyclonic shear on the northern side and a broader zone of anticyclonic shear to the south. Other studies have shown structural changes to the velocity field between crests and troughs, that is, anticyclonic and cyclonic curvature. Digitized path information (from SST images such as in Fig. 1) from which to obtain curvature of the current is not yet available, but on the assumption that crest and trough crossings have a latitudinal separation, those sections where

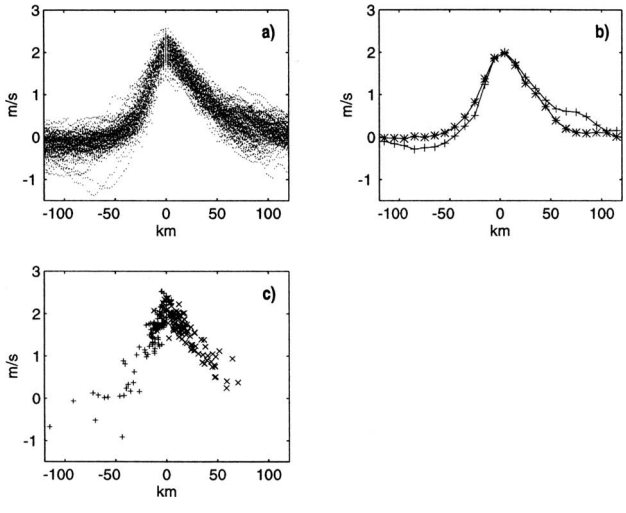

FIG. 6. Downstream velocity as defined by the direction of flow at the velocity maximum, plotted as a function of position normal to the velocity maximum vector: (a) all sections, (b) median velocity for sections north of 37.9°N (+) and south of 37.4°N (*), and (c) locations of SST maximum (×) and SST gradient maximum (+). Note the systematic shift or rocking of the velocity structure while the velocity maximum remains the same in (b).

the ship crosses v_{max} north of 37.9° (crest) or south of 37.4° (trough) are replotted in Fig. 6b. Between troughs and crests the shear vorticity increases on both sides of the current. The velocity profile sharpens on the cyclonic side and broadens on the anticyclonic side of the current. The mean latitudinal separation of 0.7° between troughs and crests implies a change in the Coriolis parameter of < 2%, much less than the shear vorticity changes observed. Between troughs and crests the curvature vorticity must decrease on both sides of the current. At 1 m s^{-1}, typical changes in curvature vorticity in the center of the current amount to -2×10^{-5} s^{-1} or –20% of f, assuming curvatures of 1/100 km, while the observed change in shear vorticity is O(30%) of f on the cyclonic side but only O(10%) on the anticyclonic side. Interestingly, the velocity field exhibits a region of low lateral shear in the 60–80-km range in meander crests. Song and Rossby (1997) observed a similar pattern in crests, albeit closer to the velocity maximum, using isopycnal floats in the main thermocline.

Although a quantitative discussion must await a more detailed analysis, the change in velocity structure can be given a simple explanation in terms of the vorticity tendencies taking place. To see this, consider layer potential vorticity, a dynamical tracer that is conserved in nondissipative flows. It can be written as PV $= (f + kv + \partial_n v)/D$, where the normal derivative is directed to the right of the flow and D represents layer thickness between two density surfaces. Holding D constant for the moment, decreasing curvature vorticity (kv) between troughs and crests requires an increase in shear vorticity *everywhere*, that is, a sharpening of the velocity gradient on the cyclonic side and a broadening on the anticyclonic side. From the above numbers, it appears that curvature change dominates on the anticyclonic side and shear dominates on the cyclonic side. This in turn requires a decrease in D or a divergence on the anticyclonic side, and an increase in D or convergence north of the velocity maximum in order for PV to be conserved. A 10% change in absolute vorticity requires a 10% change in layer thickness, which if it takes place over the 1–2-day transit time between a trough and a crest implies a divergence–convergence of O(10^{-6} s^{-1}). This agrees well with the divergence–convergence patterns observed using isopycnal floats in the main thermocline (Bower 1989; Song and Rossby 1997). In momentum terms, the shift in direction of the centripetal acceleration thrusts the *high velocity core* of the current to the left between troughs and crests, resulting in an increased pressure

gradient on the northern side and weakened pressure gradient on the anticyclonic side.

Satellite remote sensing of sea surface temperature has emphasized the northern thermal gradient as the locator of the Gulf Stream. The ADCP transducer temperature data can be used to determine the location of the maximum SST gradients (∂T_{max}). For simplicity the thermal north wall is defined as that point where the temperature drops 2°C below the maximum temperature (T_{max}) in the current. Using the same sections, ∂T_{max} and T_{max} are marked with a + and an ×, respectively, in Fig. 6c. The maximum temperatures cluster just south of the maximum velocity, while the thermal fronts cluster nearby to the north, with both exhibiting a loose scatter at greater ranges. That the highest temperatures tend to occur where the advection in the current is strongest makes sense. Almost certainly this reflects the flow not merely locally, but all along the current from the south. The coincidence of the thermal north wall at or just north of the velocity maximum indicates that the velocity maximum also serves as a property boundary between the stream and slope waters to the north. The sharpness of the thermal front suggests a net convergence to counteract any mixing processes that might weaken or broaden it in the downstream direction.

5. Sea level variations using geostrophy

The direct measurement of velocity offers many advantages, but given the sensitivity of the ADCP technique to errors in compass heading (and the serious navigational errors prior to the advent of GPS), confidence in the observations depends on demonstrating their accuracy and validity. A very powerful test for bias in the velocity data consists of integrating the cross-track velocity geostrophically to obtain the change in sea level between two points. Obviously the same result should be obtained regardless of whether the ship is in north- or southbound transit. There is a certain irony here, for although the direct measurement releases oceanographers from a major constraint they normally work under (the dynamic method), geostrophy is now used to affirm the accuracy of the ADCP technique. Figure 7 shows pressure, expressed in meters relative to sea level at a point near the shelfbreak, obtained by geostrophic integration, $g^{-1}\int fv \cos\alpha dx$, along the ship's track, where α represents the angle between the velocity vector and the normal to the ship's track, and f is the Coriolis parameter. The red and green curves represent south- and northbound transits, respectively. The GS shows up clearly as the O(1 m) jump while the broader slope of opposite sign elsewhere represents the westward return flows both north and south of the GS. The scatter in computed sea level at Bermuda exceeds by far the O(0.1 m) actually observed at Station "S," 12 n mi SE of Bermuda (Schroeder and Stommel 1965). This excess variability comes from a mixture of compass errors, mesoscale eddy activity, and inertial and tidal oscillations. Prior to the installation of the AGPS heading receiver, we thought that compass error played a major role in corrupting the local accuracy of the velocity measurements. While the variance has decreased since the installation of the AGPS, it appears that the compass error, while significant at 0.14 m s^{-1}/degree error, fluctuates with a timescale of a few hours, albeit occasionally longer, such that its integrated effect tends to cancel out. The same applies to tides and inertial oscillations; the semidiurnal tides, despite their > 10^3 km scale, have very weak velocities, < 0.05 m s^{-1}. In addition, to a vessel steaming at 16 kt these appear as a mesoscale process with an O(60 km) scale. Inertial motion, while more energetic with velocities on the order of 0.1 m s^{-1} (Briscoe and Weller 1984), has only O(20 km) horizontal scales of coherence in this region (Kunze 1986). Consequently, tides and inertial motion should cancel in the sea level integral. Thus, as near as can be determined, the mesoscale eddy field dominates the measured velocity variance in the Sargasso Sea. This might have been anticipated because south of ~34°N the velocity variance drops rather abruptly (Fig. 3d), an unlikely transition were tides or inertial motion significant contributors. Note that had the compass error substantially dominated, then the variance ellipses would have had their major axes aligned in the cross-track direction.

The mean and standard deviation of sea level at Bermuda for all south- and northbound transits equals 0.77 ± 0.45 m (N = 86) and 0.82 ± 0.29 m (N = 35), respectively; in both directions the standard error is 0.05 m. This agreement is most gratifying, for it suggests that all heading-dependent gyrocompass biases and transducer alignment uncertainties have been accounted for (in the mean). In addition to the small difference between the south- and northbound means, the tight fit associated with the northbound estimate with its fewer samples probably results from the stricter weather requirements for northbound transits due to

the ship's greater sensitivity to bubble drawdown when lightly loaded. Better weather implies less wave-induced accelerations on the vessel and hence smaller gyrocompass errors. Assuming for the moment that the standard deviation of the northbound sea level estimates, 0.29 m, has little remaining measurement error, how much of it can be accounted for? First, uncorrelated sea level variations at the shelfbreak contribute little to the integral in Fig. 7. The standard deviation in dynamic height relative to 2000 dbars in the slope waters amounts to 0.07 m (Sato and Rossby 1995), while deep sea pressure gauges from the northern edge of the GS show only 0.05-dbar standard deviation (Qian and Watts 1992). Kelly (1991) obtains 0.1 m in the slope waters 100 km east of the *Oleander* line. Removing 0.1 m from the Bermuda estimate still leaves $(0.29\ \text{m})^2 - (0.1\ \text{m})^2 = (0.27\ \text{m})^2$

A significant fraction of the sea level variance may come from the assumption of strict geostrophy in the GS, that is, the neglect of the centripetal term in the momentum balance. Accurate path knowledge of the GS at the time of each crossing must await analysis of AVHRR imagery, but the effect of curvature on the sea level integral can be assessed. In a meander trough the cyclonic curvature induces a centripetal force that results in a further increase in the total pressure difference across the front such that geostrophic integration will result in an underestimate. Similarly, omission of the curvature term at a meander crest leads to an overestimate of the pressure drop across the GS. Using the velocity cross sections in Fig. 6b, and assuming a curvature, k, of 1/100 km, gradient wind integration, $g^{-1}\int(fv + kv^2)\cos\alpha dx$, yields 1.00 m across the crest and 1.42 m at the trough, a very considerable range, suggesting that path curvature is essential for an accurate estimate of sea level difference across the GS. Lack of this knowledge may be a major factor in the large scatter in sea level estimates from hydrography. A detailed examination of the GS path and its curvature from AVHRR imagery will be required to resolve this.

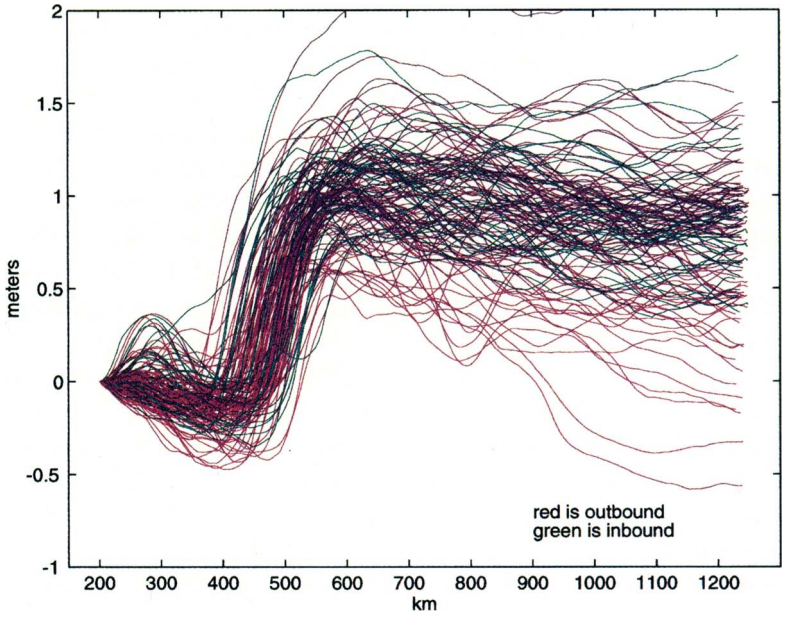

FIG. 7. Geostrophic sea level relative to 39°23′N, 72°29′W, just north of the shelfbreak, estimated from cross-track velocities from south- (red lines) and northbound (green lines) transits. The outliers (two to the south and one to the north) presumably result from a persistent compass errors of O(1°) during those transits. The mean difference and standard deviation across the GS alone equals 1.25 ± 0.21 m (N = 87) and 1.27 ± 0.15 m (N = 39) for the south- and northbound transits, respectively.

6. Sea surface temperature

The ADCP records SST continuously with time, independent of the performance of the ADCP itself. Figure 8a shows a Hovmöller (time–position) diagram of SST with distance from the New Jersey coast (40°45′N, 74°00′W) along the ordinate (subsampled to 5-km resolution) and time in years along the abscissa. Constructed from almost all biweekly transects (the pairs of black lines at certain times indicate intervals where interpolation was necessary), the bold color patterns reveal the warm and cold phases of the annual cycle, the large spread between summer and winter in the north, and the meandering of the Gulf Stream. The shelf-slope front shows up clearly in wintertime at 200 km. The bold colors of the annual cycle make it difficult to discern that some summers and winters may be warmer than others. However, by removing the corresponding 4.5-yr annual cycle from each point in Fig. 8a, the anomaly in SST can be seen clearly in Fig. 8b. Much of year 1994 emerges as a warm period throughout the region, while winter 1995 is warm only north of the GS with the Sargasso Sea significantly cooler than normal. Cold SSTs are evident north of the GS in winter 1993 and throughout all of 1996 and into 1997. Note also that the shelf-slope front,

clearly visible in the SST field, essentially disappears in the anomaly field.

The meandering of the GS over a wide range of timescales can be seen more clearly in Fig. 8c which shows the position of T_{max} in the GS. Keeping in mind that there is some scatter between the position of v_{max} and T_{max}, we see that this panel reflects the N–S trends of v_{max} in Fig. 5b quite well, but the larger data density permits a more detailed analysis. The thin and thick lines represent the 3-month and 1-yr low-pass filtered time series, respectively. On the longest timescales the stream shifts N–S nearly 100 km while the short-term meandering has an amplitude of 50–100 km. Figures 8a and 8b indicate sharper temperature gradients along the northern edge of the current than the southern. In wintertime these gradients can on occasion exceed more than 8°C in 2 km. Also, compared to the relatively uniform temperatures in the Sargasso Sea, the slope waters evince at all times of the year more variability as well as a cross-sea mean temperature gradient. The interannual variation in SST, particularly in wintertime in the slope waters, represents the strongest low-frequency variation in the *Oleander* dataset. Interestingly, the slope water SST variation (Fig. 8b) shows a correlation with GS position (Fig. 8c); specifically, warm SSTs occur when the GS is closer to the shelf (distance < about 450 km), while cold SSTs occur when it is farther south (> 450 km). A possible mechanism for this could be that an increased influx and admixture of cold shelf water into the slope water forces the GS southward and causes the cold SSTs, while a lessened influx allows the GS to move northward, resulting in warm SSTs.

7. Low-frequency variability of the surface transport

One of the most striking aspects regarding the GS to emerge from the *Oleander* dataset is the considerable stability of the directly measured surface transport over the 4.5 yr of sampling reported here. The surface transport is defined as the flow across the ship track between two points defined by where the cross-track velocity drops to zero. In order to sharpen up the low-frequency signal, the annual signal is removed; this and a least square fit are shown in Fig. 9a. The transports after removing the annual fit are shown in Fig. 9b, along with the computed mean and standard

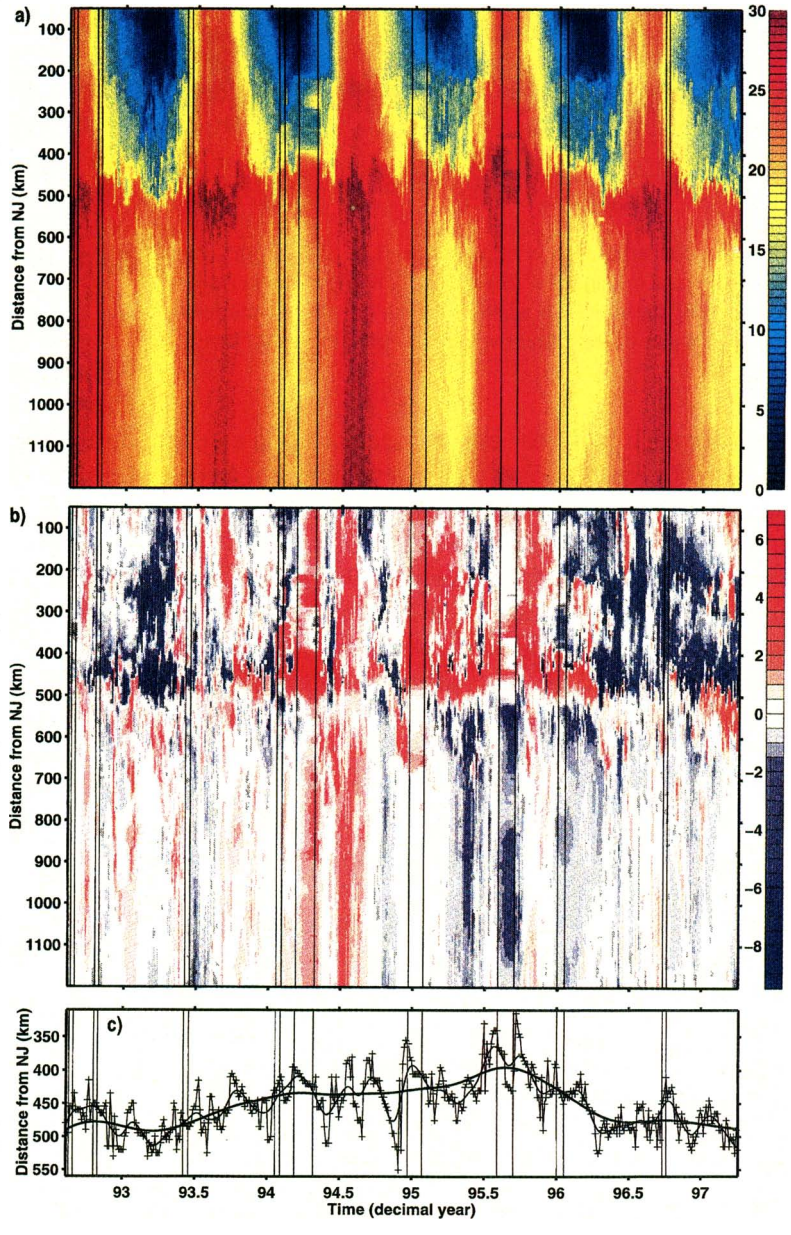

FIG. 8. (a) Hovmöller diagram of SST (°C) as a function of time (x axis) and distance from the New Jersey coast (y axis). The vertical bands correspond to the annual cycle of heating and cooling, and the wobbly warm band represents the GS and its meandering. A stable thermal front near 220 km represents the shelf-slope front. (b) Same as (a) after removal of the average annual cycle. (c) Plot of the position of the north wall of the GS, the same low-pass filtered with a 3-month and a 1-yr Butterworth filter (thin to thick lines).

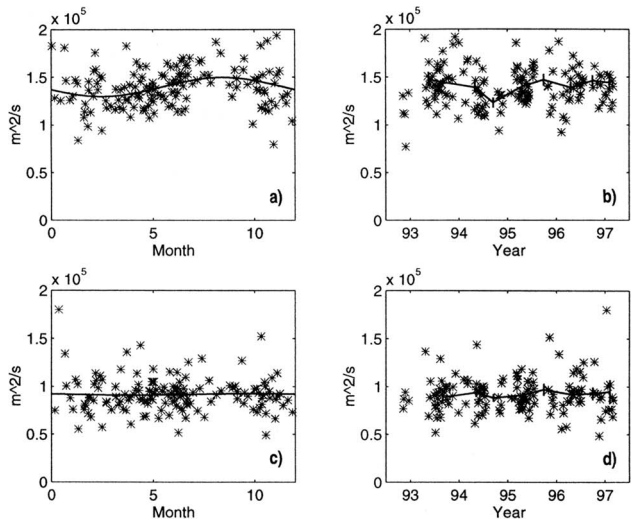

FIG. 9. Surface transport per meter depth at 52-m depth versus month [(a) and (c)] and year [(b) and (d)]. The top two panels show transport by the entire GS whereas the bottom two are limited to the central part of the current where the speed exceeds 1 m s^{-1}.

error for each half-year bin. No secular trend can be discerned over the 4.5-yr record available, but a conspicuous 0.2×10^5 m^2 s^{-1} (15%) decrease in surface transport appears to have taken place in late 1994 with rapid recovery in the following year. The corresponding change in dynamic height difference associated with such a drop would be about 0.2 dyn m, a considerable change. Since this substantially exceeds the seasonal range in dynamic height difference, it seems likely that it results from variations in either or both the main thermocline depth (Sato and Rossby 1995) and the barotropic pressure field (Qian and Watts 1992).

Recalling the stability of the velocity maximum in the GS and the tight envelope of velocities in the central part of the current (Fig. 6), the downstream transport is recomputed but limited to that part of the current where the speed exceeds 1 m s^{-1}. This emphasizes the inertial portion of the current and deemphasizes its interactions with the surrounding eddy field. The results are shown in Figs. 9c and 9d. The annual cycle all but disappears. The transport during the 4 yr, averaged in half-year bins, becomes much more stable, suggesting that it remains effectively constant to within the standard error of the estimates, about 3%–5% of the mean. Nor is any longer, secular trend evident. This indicates that the surface transport drop in 1994 (Fig. 9b), if real, was due to interactions between the low velocity field on both sides of the current and the surrounding mesoscale eddy field, but at this point no attempt has been made to examine these interactions more closely. Rapid fluctuations most likely result from the meandering itself, while longer ones may indicate regional variations in the intensity of the recirculation fields adjacent to the current. As seen in Fig. 3, there are significant pattern variations on annual timescales. These affect the recirculation fields significantly, but not the high velocity core of the current. The fact that the maximum velocity, surface integral of the high velocity core, and width (not shown) of the core have remained stable to within a few percent over 4 yr is a very significant result. Many authors have remarked on the structural stability of the GS. To this we can now add its temporal stability.

8. Poleward temperature flux

Heat flux depends of course on both the velocity and temperature fields. We have shown that the core transport shows very little variation in time, at least during this observation period. The surface temperature, on the other hand, shows a highly repeatable cycle. Figure 10 shows T_{max} in the center of the GS as a function of time. The summertime maxima all peak close to 29°C. The wintertime minima show greater variation, particularly this past winter (1997), appeared to be significantly milder. Nonetheless, the annual cycle of T_{max} in the GS varies significantly less than SST to either side of the GS. This probably results from the rapid advection of GS waters from the large warm water reservoir of the Caribbean Sea. The sur-

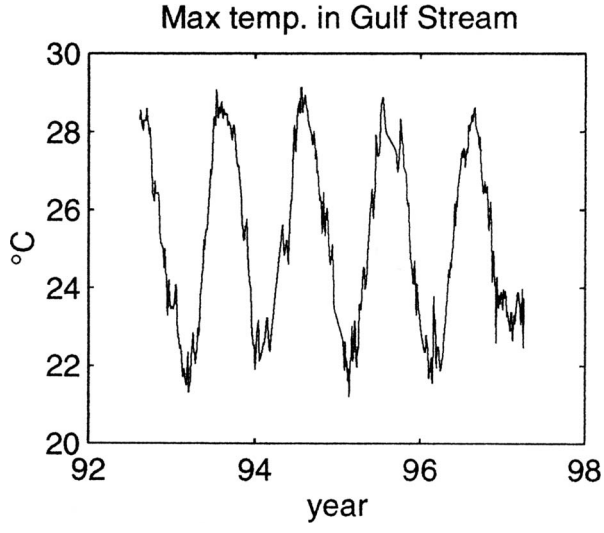

FIG. 10. T_{max} in the center of the GS as a function of time. Note the greater variations between winters than summers.

rounding water SSTs reflect variations in heat losses to the air masses blowing off North America. What are the poleward heat flux consequences of a change in temperature or transport in the GS?

Consider first the case where the volume transport is constant and the surface layer temperature varies from one year to another. Specifically, assuming that inter-winter variations of 1°C extend as deep as 100 m in wintertime and the surface transport in Fig. 9d characterizes the top 100 m as well, the corresponding heat flux change would be 0.9×10^5 m^2 s$^{-1} \times 100$ m $\times$ 1°C $\times 4 \times 10^6$ J m^{-3} = 0.036 PW. This corresponds to an O(4%) change in net heat flux at these latitudes, a small but not insignificant change. Estimates for net poleward heat flux at the latitude of the *Oleander* section (around 36°N) vary from 0.8 PW (Roemmich and Wunsch 1985) to 1.38 PW (Rago and Rossby 1987). The expendable bathythermograph (XBT) sections across the GS have been taken on a monthly basis throughout this program and will be used to examine the heat storage and upper-ocean temperature fluxes in detail.

Suppose instead that the temperature field is constant while the transport changes. Some interannual change has been noted; particularly in the latter half of 1994, the surface transport may have undergone an O(15%) decrease. On longer timescales Sato and Rossby (1995) suggested that a 6-Sv decrease in baroclinic transport might have taken place between the late 1950s and the early 1970s. While it now appears that these changes may reflect variations in the strength of the eddy continuum adjacent to the GS rather than the oceanwide circulation, let us for the moment suppose that the latter applies. The heat flux consequences of a transport change while holding temperature constant depend upon the temperature of the returning waters, that is, whether they return via a shallow primarily wind-driven path or a deep convectively driven path. For the former, the warm upper-ocean waters (20°C) might cool off to 15°C in the southward-flowing deep mixed layer of the eastern Atlantic. For the latter, the waters flow south in the Gulf Stream undercurrent with a temperature of about 2°C. A 6-Sv change in transport would result in a 6×10^6 m$^3 \times (20 - 15)$°C $\times 4 \times 10^6$ J m^{-3} ~0.12 PW and 6×10^6 m$^3 \times (20 - 2)$°C $\times 4 \times 10^6$ J m^{-3} ~0.43 PW heat flux change, respectively. These very large numbers indicate the importance of knowing the transport accurately, but they also emphasize the necessity of knowing where the heat ultimately is lost to the atmosphere, that is, the relative strengths of the wind-driven and thermohaline modes of circulation.

9. Energetics

The variance ellipses in Fig. 3 reveal the large variability due to the meandering of the GS relative to the surrounding waters. This concentrated eddy activity reflects, as many authors have noted, the meandering of the relatively robust structure of the GS itself. As the fixed velocity structure meanders, the velocity in the downstream direction increases and decreases dramatically compared to that of the cross-stream component, hence the sharp ellipticity of the variance ellipses in the GS.

While it is beyond the scope of this survey to go into a detailed discussion of instabilities in the GS, several studies (Hall 1986; Rossby 1987; Cronin and Watts 1996) suggest that both baroclinic (BC) and barotropic (BT) mean-to-eddy energy conversion may be important. The traditional estimators of these are

$$\mathrm{BC} = \langle v'\rho' \rangle \frac{\partial \overline{\rho}}{\partial z} \Big/ \frac{\partial \overline{\rho}}{\partial z} \rho_0 \approx -\alpha g \langle v'T' \rangle slope(\rho')$$

and

$$\mathrm{BT} = -\frac{\partial \langle u \rangle}{\partial y} \langle u'v' \rangle,$$

where ρ is the density of water, α the coefficient of thermal expansion, g gravitational acceleration, and x and y the mean down- and cross-stream directions, respectively.

To estimate BC properly requires information on the density field, which unfortunately is obtained only on a monthly basis from concomitant XBT sections. However, since the cross-stream structure has proved to be quite robust, we can use the mean slope of the isopycnals (~0.01) instead (in the second right term in BC above). The rest of BC is readily evaluated. We use the ADCP temperature to evaluate T', keeping in mind that while the absolute temperatures do not matter, its variance may be somewhat large due to the shallow 5-m depth of the measurements. (The T' used corresponds to the residuals in Fig. 8b, i.e., after removal of the annual cycle.) The cross-stream component v' has been shown to be fairly depth insensitive (Halkin and Rossby 1985). The results (dashed lines) are shown in Fig. 11 for the same periods as the mean fields in Fig. 3. Analogous to BC, BT represents the transfer of momentum between the mean flow and

eddy field. Their statistics are also shown in Fig. 11 (solid lines). The yearly subsets make it clear that considerable interannual variability in both conversion terms exists. The BT term remains strong on the cyclonic side but is more variable on the anticyclonic side. The 4.5-yr average shows two maxima (the southern one weaker), which appear to be qualitatively similar to those of the Hall, Rossby, and Cronin and Watts papers cited above. The magnitude of the BC term is larger than theirs probably because of the shallow depth (52 m for v' and 5 m for T') compared to 400 m in the Cronin and Watts study.

10. Discussion and summary

This ADCP program on the M/V *Oleander* in weekly service between Bermuda and New Jersey has been in continuous operation since fall 1992. The technical issues, of which there were many, have recently been discussed (Flagg et al. 1998). The equipment down time has been gratifyingly little, about 28 weeks (including 8 weeks for drydocking) during the 4.5-yr program reported here. This speaks well for the use of volunteer observing vessels for systematic observations of ocean currents and other parameters that can be monitored on an unattended basis (Rossby et al. 1995). In this program the major observational limitation has been the frequency of bubbles underneath the vessel due to its flat bottom and shallow draft. This limitation notwithstanding, the accumulated dataset is unique in its continuity and length of coverage of the GS and the NW Atlantic. The primary objective of the program has been to examine and quantify the structure and variability of the upper-ocean transport and its role in poleward heat transport in the North Atlantic. In this regard the message to date has been an unexpected one: the surface transport appears to be astonishingly stable. The variability that oceanographers have observed from hydrographic observations appears to result from two factors: 1) not having curvature information in the transport integration and 2) changes in the strength and intensity of the recirculations to either side of the GS. The surface transport in the central part or core of the GS, defined as where the speed is greater than 1 m s^{-1}, remains remarkably constant, independent of season and year. To put this in a larger context, the transport of all waters moving at speeds > 1 m s^{-1} sums to somewhat more than 20 Sv. Similarly, the maximum velocity in the GS shows quite unexpected stability. While 2 m s^{-1} (4 kt) has often been quoted as the characteristic speed of the center of the current at the surface, a standard deviation of 0.24 m s^{-1}, regardless of position, direction, curvature, season, or year, and including the effects of GPS dithering and instrument measurement error, is smaller than we had expected. It is assumed that the observed scatter is associated with local variability embedded within the meandering of the current, certainly not low-frequency temporal variations. The stability of the velocity maximum suggests that the GS tends to adjust the density more than the velocity field.

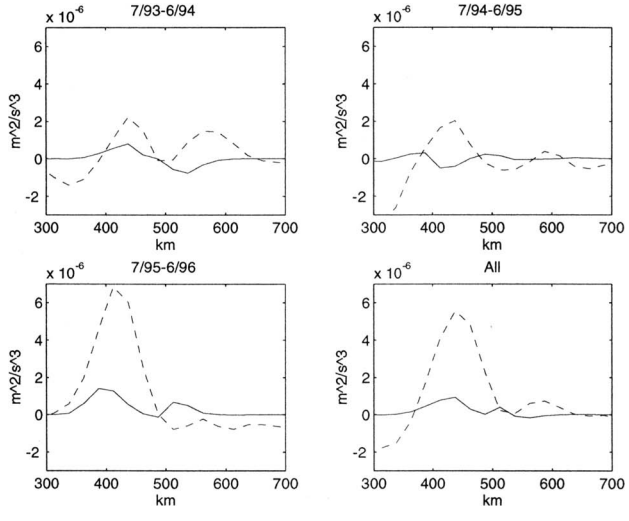

FIG. 11. Baroclinic (dashed) and barotropic (solid) conversion rates as a function of distance for the periods corresponding to the mean fields in Fig. 3.

Perhaps the stability of the core transport is not surprising if it is thought of as resulting from the large-scale wind-driven and thermohaline circulations with their wide-area driving forces. More than 20 yr of cable measurements in the Florida Straits show an annual range in transport of 3.2 Sv (around a 32.3-Sv mean) but no long-term trend (Larsen 1992). More distantly, but as a measure of the intensity of the thermohaline mode, Dickson and Brown (1994) note that the overflow of waters through the Denmark Straits appears to be quite stable despite documented changes in deep convection patterns in the Nordic Seas.

The variations in transport that do occur seem to be associated with the regional scale. This can be seen from Fig. 3, which shows the mean and variance patterns from 3 years. While the GS shows up very clearly, the shape of the return flows to either side indicate significant variations on scales of several hundred kilometers and timescales of many months. Kelly (1991) has made a similar inference from GEOSAT

(Geodetic Earth Orbiting Satellite) altimeter observations of sea level. Similarly, the baroclinic and barotropic energy conversion terms show significant interannual variations, but we have not yet attempted to correlate these with the observed circulation changes. Recently, Spall (1996) has proposed a feedback mechanism between upper deep western boundary current (DWBC) and the GS such that the eddy fluxes that drive the recirculation gyres depend upon mean potential vorticity field supplied by the DWBC, which in turn can modify the eddy fluxes. According to his model results, the process appears to have a decadal period. To the best of our knowledge the meandering intensity shows no "decadal" variability. Lee and Cornillon (1995) in their analysis of 8 yr of Gulf Stream images made no comment about secular or decadal trends. Nonetheless, the Spall or similar mechanisms might operate on a regional scale. The *Oleander* line crosses the GS just west of where it often develops a steep trough. As the trough waxes and wanes, so also may the rate of expulsion of low vorticity waters vary, thereby altering the intensity of the recirculation locally. Consistent with the conclusions of many other studies, the GS appears to be baroclinically unstable although the rate of mean potential to eddy kinetic energy conversion varies significantly with time. These are issues that the *Oleander* dataset, together with regional AVHRR and sea level information, should be able to address in detail.

The repeat sections also indicate a systematic shift in the velocity structure as it meanders north and south. In crests the lateral shear is systematically greater (more positive) than in troughs. The fact that the increase in shear undercompensates for curvature change on the anticyclonic side and overcompensates on the other requires, if potential vorticity is to be conserved, divergent and convergent flow south and north of the velocity maximum, respectively. This inference is consistent with earlier deductions about divergence patterns using isopycnal floats (Bower 1989; Song and Rossby 1997). Once the path of the GS and its curvature in the vicinity of the ship crossing have been obtained from AVHRR imagery, these observations will be analyzed in detail.

The north–south displacement of the velocity maximum has been noted in a number of studies (Lee and Cornillon 1995; Kelly 1991). The former study, which spans almost 8 years of AVHRR data (April 1982–December 1989), shows a well-defined annual range of ~40 km in displacement between 75° and 60°W with significant interannual variations ranging from 30 to 60 km. These shifts exceed the ~20 km displacements observed here, almost certainly because the New Jersey–Bermuda line intersects the GS close to where it has a node in its meandering envelope (Cornillon 1986). The cause of this north–south migration of the GS has not been established, but almost certainly it is related to the depth variations of the main thermocline in the Sargasso Sea if the volume of 18°C water is to be conserved. A 25-m annual cycle in the depth of the 800-m-deep main thermocline (Sato and Rossby 1995) means a 5% stretching, which translates into an O(20 km) change in N–S width for a 500-km-wide recirculation gyre, that is, comparable to that observed.

To conclude on a practical note: these VOS observations of the GS highlight the value of 1) direct observations of velocity and 2) repeating them systematically over a long period of time. It is our hope that these observations, by themselves and in combination with AVHRR and Topography Experiment (TOPEX) altimetry (which overlaps perfectly with this observation program) will lead to a deeper understanding of the GS and its machinery.

Acknowledgments. First and foremost we must express our appreciation and thanks to Mr. Cor Teeuwen of the Bermuda Container Lines for his interest and enthusiastic support of this project. From the very start, he has taken a keen interest in the project and has when and wherever possible offered suggestions on how to make the program as successful as possible. Dr. C. Flagg at the Brookhaven National Laboratory played the major instrumental role in adapting the ADCP technology for automated operation on board the M/V *Oleander.* Mr. George Schwartze has played a crucial role in implementing and maintaining the high standard of operation onboard. Our colleagues at the National Marine Fisheries Service, Narragansett, Rhode Island, provided the initial contact with the M/V *Oleander* and have been a pleasure to work with in sharing the burden of travel to/from Port Elizabeth, and the regular supervision of the equipment. Prof. Eric Firing at the University of Hawaii and Mr. John Ryan here at GSO have provided valuable help with the debugging of some of the vexing data quality issues. Mrs. S. Anderson-Fontana graciously helped us through some difficult times with very welcome assistance with the data processing. We particularly want to express our gratitude to Drs. D. Goodrich and J. Todd of the Office of Global Programs, NOAA, for their continued confidence and support. The program is funded by NOAA OGP Contracts NA16RC0523 and NA56GP0220.

References

Bower, A. S., 1989: Potential vorticity balances and horizontal divergence along particle trajectories in Gulf Stream meanders east of Cape Hatteras. *J. Phys. Oceanogr.,* **19,** 1669–1681.

Briscoe, M. G., and R. A. Weller, 1984: Preliminary results from the Long-Term Upper Ocean Study (LOTUS). *Dyn. Atmos. Oceans,* **8,** 243–265.

Cornillon, P., 1986: The effect of the New England Seamounts on Gulf Stream meandering as observed from satellite IR imagery. *J. Phys. Oceanogr.,* **16,** 386–389.

Cronin, M., and D. R. Watts, 1996: Eddy–mean flow interaction in the Gulf Stream at 68°W: Part I: Eddy energetics. *J. Phys. Oceanogr.,* **26,** 2107–2131.

Dickson, R. R., and J. Brown, 1994: The production of North Atlantic Deep Water: Sources, rates and pathways. *J. Geophys. Res.,* **99** (C6), 12 319–12 341.

Flagg, C., G. Schwartze, E. Gottlieb, and T. Rossby, 1998: Operating an acoustic Doppler current profiler (ADCP) onboard a container vessel. *J. Atmos. Oceanic Technol.,* **15,** 257–271.

Greatbatch, R. J., A. F. Fanning, A. D. Goulding, and S. Levitus, 1991: A diagnosis of interpentadal circulation changes in the North Atlantic. *J. Geophys. Res.,* **96** (C12), 22 009–22 023.

Halkin, D., and T. Rossby, 1985: The structure and transport of the Gulf Stream at 73°W. *J. Phys. Oceanogr.,* **15,** 1439–1452.

Hall, M. M., 1986: Horizontal and vertical structure of the Gulf Stream field at 68°W. *J. Phys. Oceanogr.,* **16,** 1814–1828.

Hogg, N. G., 1992: On the transport of the Gulf Stream between Cape Hatteras and the Grand Banks. *Deep-Sea Res.,* **39,** 1231–1246.

Johns, W. E., T. J. Shay, J. M. Bane, and D. R. Watts, 1995: Gulf Stream structure, transport and recirculation near 68°W. *J. Geophys. Res.,* **100,** 817–838.

Kelly, K. A., 1991: The meandering Gulf Stream as seen by the Geosat Altimeter: Surface transport, position, and velocity variance from 73°W to 46°W. *J. Geophys. Res.,* **96,** 16 721–16 738.

Knauss, J., 1969: A note on the transport of the Gulf Stream. *Deep-Sea Res.,* **16** (Suppl.), 117–123.

Kunze, E., 1986: The mean and near-inertial velocity fields in a warm-core ring. *J. Phys. Oceanogr.,* **16,** 1444–1461.

Larsen, J. C., 1992: Transport and heat flux of the Florida Current at 27°N derived from cross-stream voltages and profiling data: Theory and observations. *Philos. Trans. Roy. Soc. London,* **228A,** 169–236.

Lee, T., and P. Cornillon, 1995: Temporal variation of meandering intensity and domain-wide lateral oscillations of the Gulf Stream. *J. Geophys. Res.,* **100** (C7), 13 603–13 613.

Levitus, S., 1989: Interpentadal variability of temperature and salinity at intermediate depths of the North Atlantic Ocean, 1970–1974 versus 1955–1959. *J. Geophys. Res.,* **94,** 6091–6131.

Qian, X., and D. R. Watts, 1992: The SYNOP experiment: Bottom pressure maps from the central array May 1988 to August 1990. University of Rhode Island Graduate School of Oceanography Tech. Rep. 92-3, 187 pp. [Available from Graduate School of Oceanography, University of Rhode Island, Narragansett Bay Campus, Narragansett, RI 02882-1197.]

Rago, T. A., and T. Rossby, 1987: Heat transport into the North Atlantic Ocean north of 32°N latitude. *J. Phys. Oceanogr.,* **17,** 854–871.

Roemmich, D. H., and C. Wunsch, 1985: Two transatlantic sections: Meridional circulation and heat flux in the subtropical North Atlantic Ocean. *Deep-Sea Res.,* **32,** 619–664.

Rossby, T., 1987: On the energetics of the Gulf Stream at 73°W. *J. Mar. Res.,* **45,** 59–82.

——, G. Siedler, and W. Zenk, 1995: The volunteer observing ship and future ocean monitoring. *Bull. Amer. Meteor. Soc.,* **76,** 5–11.

Sato, O. T., and T. Rossby, 1995: Seasonal and low frequency variations in dynamic height anomaly and transport of the Gulf Stream. *Deep-Sea Res.,* **42** (1), 149–164.

Schroeder, E., and H. Stommel, 1969: How representative is the series of Panulirus stations of monthly mean conditions off Bermuda? *Progress in Oceanography,* Vol. 5, Pergamon Press, 31–40.

Song, T., and T. Rossby, 1997: Analysis of Lagrangian potential vorticity balance and lateral displacement of water parcels in Gulf Stream meanders. *J. Phys. Oceanogr.,* **27,** 325–339.

Spall, M. A., 1996: Dynamics of the Gulf Stream/Deep Western Boundary current crossover. Part II: Low-frequency internal oscillations. *J. Phys. Oceanogr.,* **26,** 2169–2182.